Proceedings of the 2016 International Pipeline Conference
IPC2016
September 26-30, 2016, Calgary, Alberta, Canada

IPC2016-64610

COMPARISON OF J-INTEGRAL MEASUREMENT METHODS ON CLAMPED SINGLE-EDGE NOTCHED TENSION SPECIMENS

Timothy S. Weeks, Jeffrey W. Sowards, Ross A. Rentz
National Institute of Standards and Technology
Boulder, CO, USA

David T. Read, Enrico Lucon
Protiro, Inc.
Denver, CO, USA

ABSTRACT

This paper reports an extension of a previous study that compared methods of evaluating *J* by the crack mouth opening displacement and by surface strain gradients. Here, the surface strain gradients are measured by three-dimensional digital image correlation. The results herein represent a small test matrix that involved evaluation of the *J*-integral for clamped single-edge notched tensile specimens from API 5L X65 base-metal, weld metal and the adjacent heat affected zone; the *J*-integral was evaluated by a standardized procedure utilizing the crack mouth opening displacement (CMOD) and by the contour integral method on an external surface strain contour. Digital image correlation provides sufficient full-field strain data for use by this method and is considerably more robust than surface-mounted strain gage instrumentation. A series of validity checks are presented that demonstrate that the data are useful and valuable. Experimental determination of the *J*-integral is not limited to thoroughly analyzed test geometries and may be achieved with limited instrumentation. Furthermore, the method described does not require a determination of crack size nor any instrumentation that requires access to the crack mouth.

INTRODUCTION

While a number of industry- and material-relevant test and measurement methods exist [1-5], none can precisely capture the intrinsic material property typically referred to as toughness. Notwithstanding, the various methods employed are valuable to determine and compare engineering parameters that adequately quantify the materials' toughness. The direct comparison between the methods is subject to a variety of factors that influence the results. Factors such as specimen geometry, initial notch/crack geometry and load application are typically considered to affect the results through constraint. Specifically, the limits and application of critical assumptions regarding elastic-plastic conditions at the crack-tip will influence the results of model calculations of *J*-integral values, from which factors in the test protocols are derived.

The single-edge notched tension (SE(T)) specimen has been widely used to determine fracture resistance curves for high-strength line pipe steels. The authors have been actively involved in research to compare the various test and measurement methods [6, 7]. Recent work directly compared two methods of determining the *J*-integral, first, by use of crack mouth opening displacement (CMOD) measurement, and second, by use of surface strain contour measurements [7]. Conclusions of that work indicate that the two methods result in commensurate *J*-resistance (*J*-R) curves but that the strain gradients measured did not adequately capture the large plastic strains associated with crack extensions of interest in pipeline steels, therefore limiting the range of crack extensions where *J*-R could be accurately compared between the two methods. The work referenced above measured the strain gradients by use of surface-mounted resistance strain gages. The results were promising, but showed that an improved measurement technique was needed to capture the gradients over a larger range of strain. The results presented here show that digital image correlation (DIC) meets this need.

DIC is a mature technique to determine surface displacements with sub-pixel accuracy and is relatively simple

to use. DIC provides high fidelity data sets over large areas of interest and significantly higher strain capability compared to traditional instrumentation. A number of researchers have used DIC as a measurement tool in fracture mechanics, combining measurement data with finite element analysis [8, 9] and even on SE(T) specimens [10-12]. However, the techniques referenced for SE(T) specimens use DIC on the side-face of the specimens only. While DIC is a much more involved technique as compared to simple single gauge measurements like CMOD, the goal here is to advance the use of DIC on large scale tests where access to the cross-section of a flawed feature (e.g. girth weld) or access to the crack mouth is impossible. Validation of the technique by use of small scale specimens (e.g. SE(T)) is necessary and is the focus of this paper. Furthermore, the use of CMOD to calculate *J*-integral depends on a detailed finite element analysis to include crack extension.

The experimental design including the specimen geometry and the measurement techniques are presented here along with a discussion of various measurement complexities that required validation. While the work was conducted on a welded API 5L X65 line pipe steel in which the *J*-R curve is of interest, here we present only measurement methods, analysis and results for *J*-integral values. A more comprehensive analysis of the results with respect to base-metal, weld metal centerline and heat affected zone crack growth resistance is the subject of a future paper.

EXPERIMENTAL DESIGN

The specimen blanks were sectioned from a 36 in [outside diameter (OD)] by 15.7 mm [nominal wall thickness (WT)] joint with a girth weld. The weld procedure was a low heat input, pulsed-gas metal arc weld (P-GMAW). The welding position was 5G for the root weld and 1G rolled for the hot pass, fill passes and cap pass. The procedure was designed for an over-matched weld. The average yield and ultimate tensile properties were 552 MPa 653 MPa (± 5 MPa) for base-metal (longitudinal) and 674 MPa and 733 MPa (± 1 MPa) for all weld metal (circumferential).

Square cross-section specimens ($B \times B$, $B=W$) were used. The nominal thickness (B) of each specimen was 14 mm. The initial crack-size-to-thickness ratio (a_0/W) was set at 0.35; the specimens were notched by use of wire electrical discharge machining (EDM) and were not fatigue pre-cracked. The average notch root-radius was 0.085 mm. A total of nine specimens were tested; three specimens were notched in the base-metal (BM), three specimens were notched along the weld-metal centerline (WMC) and the remaining three were notched in the heat affected zone (HAZ). Integral knife edges were also cut into the specimens by use of wire EDM. Lastly, side grooves were cut into the specimens by use of wire EDM, having a nominal depth of 0.7 mm on each side ($0.05B$ per side) and a root radius of 0.5 mm.

The specimens were clamped in hydraulic grips with a nominal grip separation of 140 mm ($10W$). Each specimen was subjected to a loading-unloading profile with six cycles in the elastic region with incremental load drops equal to 25 % of the incremental maximum load. Each loading-unloading cycle was performed in displacement control at a rate of 0.025 mm/s. Additional loading-unloading cycles were performed with the 25 % load drop until the yield transition occurred. After the transition, the load drop was fixed at 25 kN and approximately forty-five partial unloadings were performed to allow a crack size estimate from CMOD-Load unloading compliance. Prior to each partial unloading a displacement-controlled three-second hold-time was completed. Additionally, the cycle increment after the yield transition was controlled by the CMOD gauge. A relative limit of 0.05 mm on the CMOD signal triggered the subsequent hold and partial unloading. Additional details regarding the loading-unloading profiles can be found in [6]. Each test was terminated once the incremental maximum load (during re-loading) reached 80 % of the peak load recorded for that specimen.

Similar to previous studies by the authors, this study employed both test methods simultaneously on a common specimen during the conduct of a test. This unambiguously normalizes critical test parameters (i.e., material, geometry, instrumentation, environment, and operator) between the methods, and is the principal enabler for direct comparison of the two methods.

INSTRUMENTATION

A full-bridge ring-style CMOD gauge was installed on each specimen by use of integral knife edges. The CMOD gauge signal was used with the UC (unloading compliance) method to determine the total crack size during the test. Again, the crack size is necessary for the calculation of *J* from the CMOD but is not required for calculation of *J* from strain gradient contours.

To capture the strain gradients during the test, each specimen was prepared with a random speckle pattern for the DIC measurement system. Two cameras were used to capture three-dimensional (3D) deformation information. While only planar data is necessary for the current measurement method, the additional data may prove useful and are the subject of ongoing analyses. Two faces of the specimen were speckled and recorded throughout the test: the back-face (opposite the notch and CMOD gauge) and one side-face. Figure 1 shows a typical speckle pattern with the double-clip gauge fixture attached. The clip gauge visible in the photo is not the CMOD clip gauge, which was installed in the integral knife edges. These tests included the double-clip gauge method in addition to the CMOD gauge, but those results are not reported in this paper.

The images contained 3248 by 4872 gray-scale pixels, of which an area of interest approximately 300 by 1000 pixels was

analyzed, yielding approximately 16 pixels per millimeter. The two cameras were aligned axially with each specimen and had an included angle of 25 degrees between cameras. The specimens were viewed at 45 degrees from each speckled face. The DIC was carried out by a commercial software application on subsets approximately 25 pixels square. Different analysis options and parameters were evaluated to arrive at the best possible correlation coefficients. Uncertainties associated with speckle patterns and analysis details will be discussed in the Discussion section.

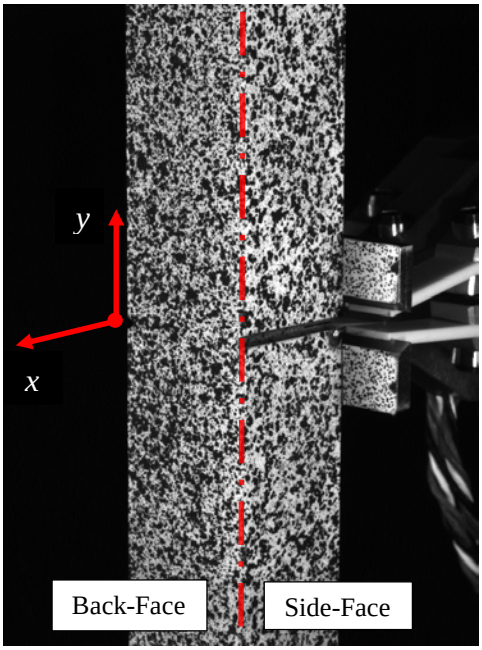

Figure 1. Pre-test photograph showing painted speckle patterns on the back-face and side-face of the specimen. Also shown in view is the speckle pattern applied to the double-clip gauge fixture. The coordinate system is chosen such that the crack extends in the *x* direction.

DIC targets applied to the back of the double-clip gauge fixtures allowed a check that the DIC measurement could replicate the CMOD measurement; in one of our tests these CMOD data were used to establish the synchronization between the DIC images and the force data.

As stated, the targets applied to the double-clip gauge fixture were used to measure the displacement between the targets. Since the double-clip gauge fixtures were rigidly mounted to the front-face (notched side) of the specimen, the displacement measured by use of these targets should reproduce the CMOD data. Figure 2 shows DIC displacement ($CMOD_{DIC}$) plotted against the CMOD signal ($CMOD_m$). A perfect correlation would result in a straight line with a slope of one. Least squares fitting of the data resulted in a slope of one as shown in Figure 2, however, more careful examination of the data yielded an uncertainty of 0.3 % with slightly diverging errors with increasing CMOD. The targets proved to be useful to avoid possible effects of local deformation as well as difficulties with obtaining a good correlation very near the edge of the specimen with the camera angle of 45 degrees from this face.

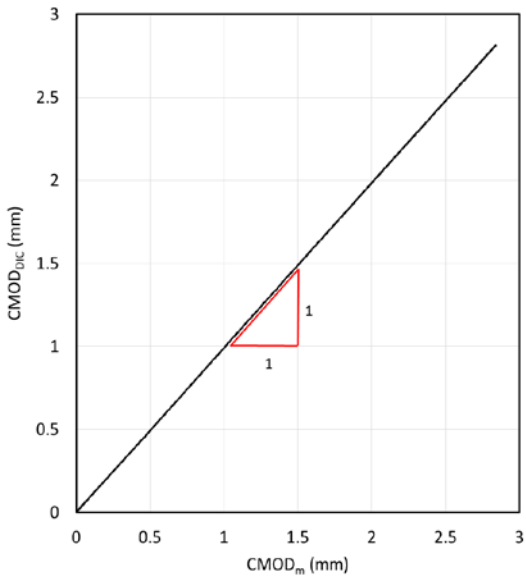

Figure 2. Plot of CMOD from DIC vs. the clip gauge measured CMOD at the integral knife edges.

The next validity check was to ensure that the DIC strain measurements were providing the anticipated strain gradients along the back-face. Figure 3 shows the axial strain within the defined areas of interest showing the asymmetric strain gradient experienced during the test of a specimen notched in the heat affected zone of the weld.

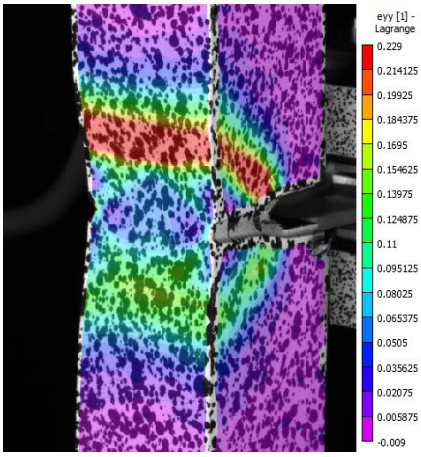

Figure 3. Axial strain pattern showing the asymmetric strain gradient experienced during the test of a specimen notched in the heat affected zone on the upper side of the weld. The lower axial strain in the weld metal is expected because the weld is overmatched.

Base-metal specimens exhibited much more symmetric strain gradients along the back-face; an example is shown

graphically in Figure 4. The different curves correspond to images obtained at increasing CMOD values. Additional back-face strain plots are shown in Figure 5 and Figure 6 for a specimen notched along the weld-metal centerline and a specimen notched in the heat affected zone, respectively. It is obvious from these figures that asymmetry increases for specimens with notches in the heat affected zone. While this is anticipated, it complicates the analysis considerably and will be discussed further in the Analysis and Discussion sections.

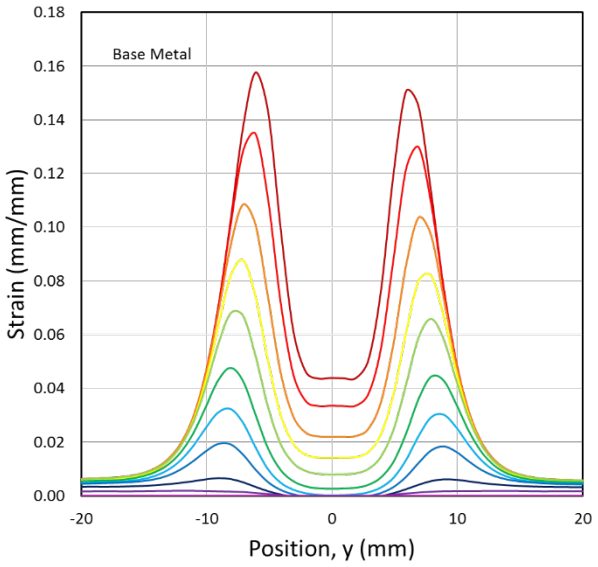

Figure 4. Plot of axial strain vs. position about the notch plane (y=0) for a base-metal specimen. The different curves are for increasing values of CMOD.

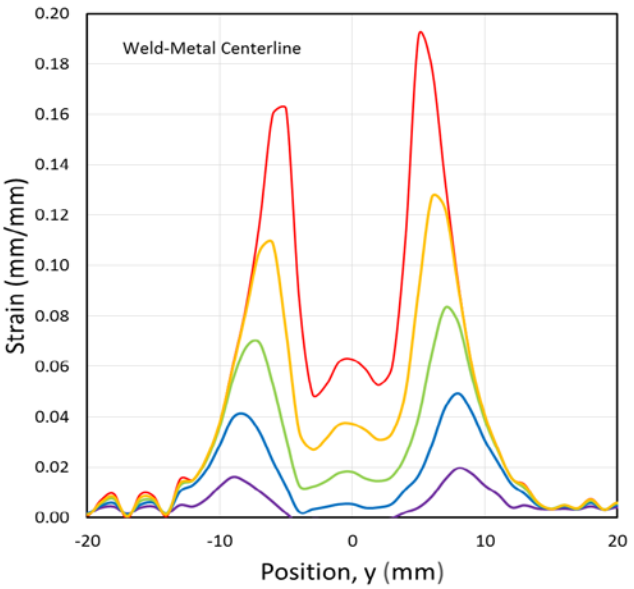

Figure 5. Plot of axial strain vs. the position about the notch plane (y=0) for a specimen notched along the weld-metal centerline. The curves are for increasing values of CMOD.

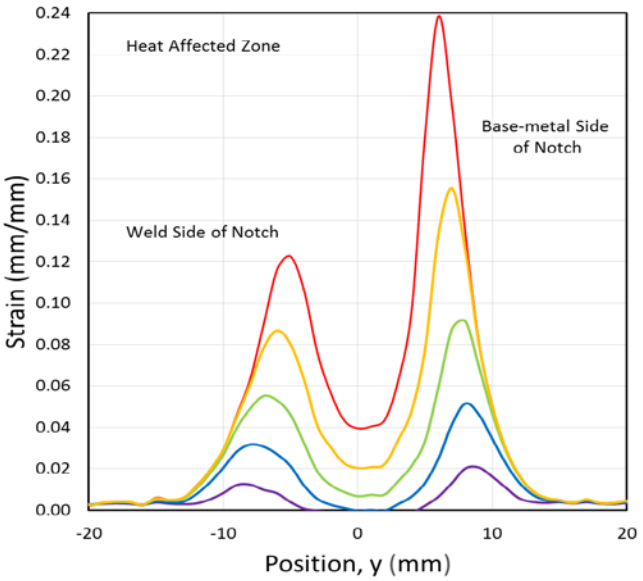

Figure 6. Plot of axial strain vs. the position about the notch plane (y=0) for a specimen notched in the heat affected zone of the notch. The curves are for increasing values of CMOD.

ANALYSIS

For comparative purposes, J from CMOD is calculated by the finite element analysis (FEA) based eta-factor. The method used here follows the guidelines proposed by Shen et.al. [13] with a notable difference in the calculation of a_i/W provided from [14].

The analysis procedures using strain gradients to calculate J have been published previously [7], with noted differences below. The salient concept is that a direct implementation of Rice's [15] reported mathematical definition of J can be used with the strain data obtained herein. From Rice,

$$J = \oint_{\Gamma} \left(W_{\varepsilon} dy - \vec{T} \cdot \frac{d\vec{v}}{dx} ds \right), \qquad (1)$$

where x and y are position coordinates, as shown in Figure 1. W_{ε} is the strain energy density function, $\vec{T}$ is the normal traction vector, (force vector per unit area), $\vec{v}$ is the full displacement vector, and ds is an element of arc length along the contour (Γ). Here we reduce the dot product to the y-direction part $T_y v_y$, this is possible because x and z contributions are zero.

A reference function giving the strain energy density as a function of axial true strain was determined from the uniaxial stress-strain data.

$$W(\varepsilon) = \int_0^{\varepsilon} \sigma_{uss} d\varepsilon_{uss} , \qquad (2)$$

where, σ_{uss} and ε_{uss} are the true-stress and true-strain values from the uniaxial stress-strain curve for this material. It is noteworthy here that several methods of determining stress from DIC strain are possible and several different treatments of the strain data are also possible that will affect the results considerably. These differences and their complexities will receive special attention in the Discussion section.

Recall that Rice's original mathematical definition of *J* assumes a closed contour, where the first difference in the present method from that used previously occurs. Specifically, here only the back-face strain gradients were used in calculating the strain energy density. The contribution of the front-face strains to *J* is negligible, as shown below in the Discussion section, and is therefore ignored.

The second term of the *J* definition (Eq. 1), applicable to the transverse segments of the contour, was approximated by the product of the average tensile stress and the difference in axial displacement from the front-face (v_1^s) to the back-face (v_2^s); this relationship is shown in Eq. 3,

$$-\int_{\Gamma} T_y \frac{dv_y}{dx} ds = \frac{P}{A}(v_1^s - v_2^s). \quad \textbf{(3)}$$

As was previously noted [7], if dv_y/dx is constant through the specimen from the front-face to the back-face, no error is encountered in the approximation of T_y as the magnitude of the average tensile stress. This assumption is easily checked as shown in Figure 7. Another difference from our previous experiments is that dv_y/dx is evaluated from the side-face DIC data as opposed to the extensometers used previously. To be clear, previously the extensometers were installed along the axial centerline of the specimen whereas here the side-face DIC data is measured. This offsets the measurement from the axial centerline of the specimen by the half-width.

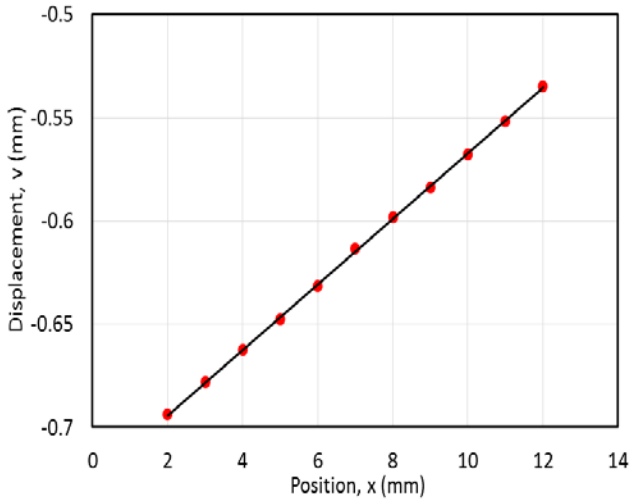

Figure 7. Plot of y-direction displacement vs. position (back to front, across the side face), derived from the side-face DIC data, 50 mm from the notch plane. A straight line indicates a constant dv_y/dx, allowing for the average stress in the remaining ligament to be used in the traction- bending term for the *J*-integral.

RESULTS

The comparisons of *J* between the two methods presented here begin with plotting the values of *J* from the two measurement methods against the CMOD value. These comparisons are shown in Figure 8 for base-metal specimens, Figure 9 for specimens notched in the weld-metal centerline and finally in Figure 10 for specimens notched in the heat affected zone of the weld. Remarkably, the J_{CMOD} data for all the welded specimens (WMC and HAZ) were graphically indiscernible among the specimens as shown in Figure 11 with only slight differences between the welded specimens and the base-metal specimens.

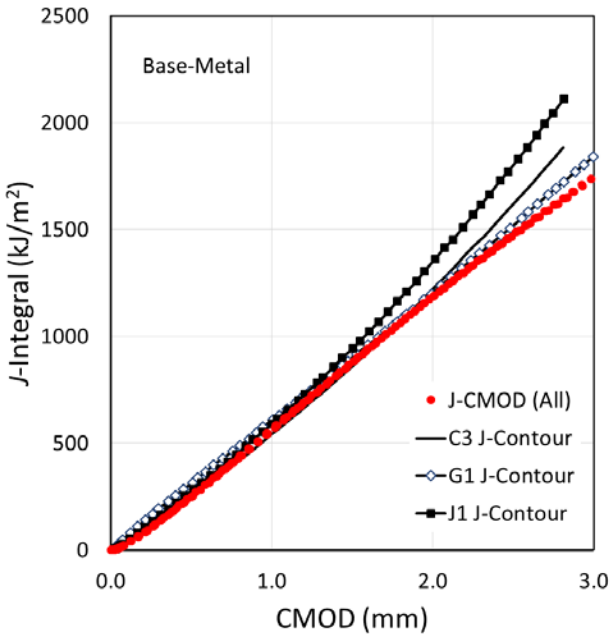

Figure 8. Comparison plot of *J* vs. CMOD for base-metal specimens. $J_{Contour}$ data for specimens C3, G1 and J1 are separated in the legend, where J_{CMOD} data for each specimen are not distinguishable.

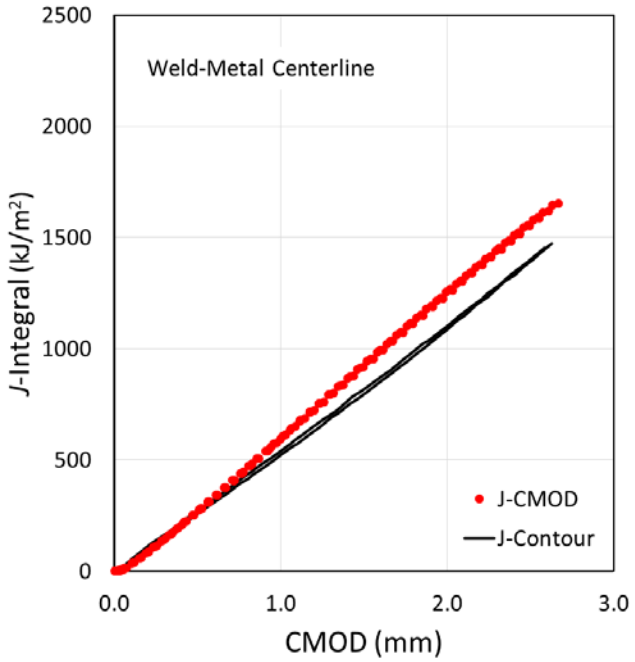

Figure 9. Comparison plot of *J* vs. CMOD for all specimens notched along the weld-metal centerline.

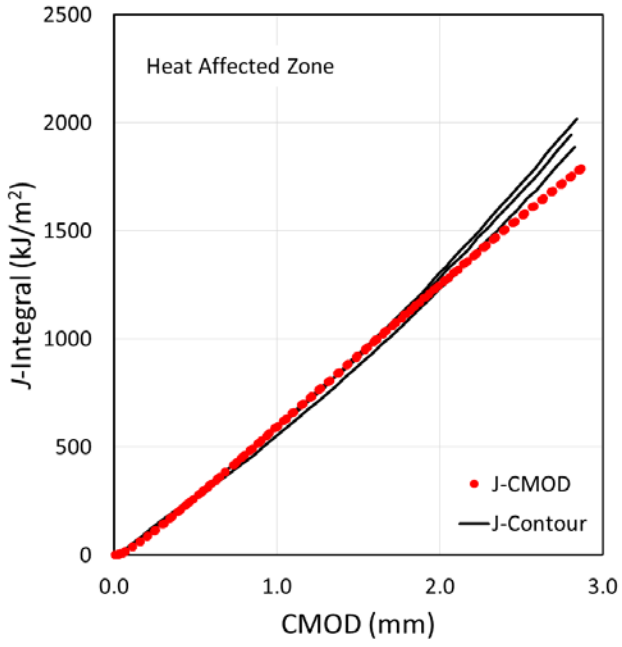

Figure 10. Comparison plot of *J* vs. CMOD for all specimens notched in the heat affected zone of the weld.

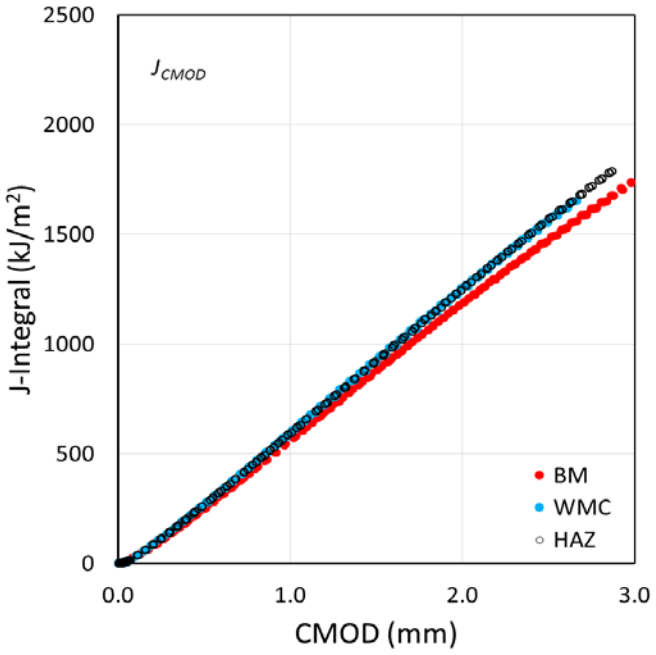

Figure 11. Comparison plot of J_{CMOD} vs. CMOD for all specimens tested. Note that the WMC and HAZ notches fall on a single curve, slightly above the base metal curve.

DISCUSSION

Simple measurement validity checks have been implemented and are shown earlier in Figure 2 and Figure 7. These ensure that the DIC system and the techniques applied here can be trusted, and at very least, no significant technical problems with the method precluded its application here.

There is no doubt that much research effort has been spent on determining *J* from CMOD and a number of researchers have proposed modifications to the calculations but in the interest of comparisons here, using CMOD data to calculate *J* shall be regarded as the reference for our purposes. The specific details of the calculation can be found in [2], with a small difference in the equation to calculate the incremental crack size using a reduced number of terms as is given by Cravero et.al. [14].

The simplest comparison between the two methods begins with examining data from base-metal specimens. Referencing Figure 11, it is clear that J_{CMOD} is quite consistent with very little scatter. From Figure 8 comparing $J_{Contour}$ to J_{CMOD} it is clear that there are differences between $J_{Contour}$ and J_{CMOD}, larger scatter among the specimens, and, particularly noteworthy, the non-linear upward trend of *J* with increasing CMOD.

Recalling that there are two terms in Rice's definition of *J*, we first examine which of these terms is subject to the most significant increases as CMOD and ultimately net section plasticity increases. Plotting both of these terms independently against CMOD clearly shows that the strain energy density term (first term) of Rice's definition will receive all of our effort, see Figure 12.

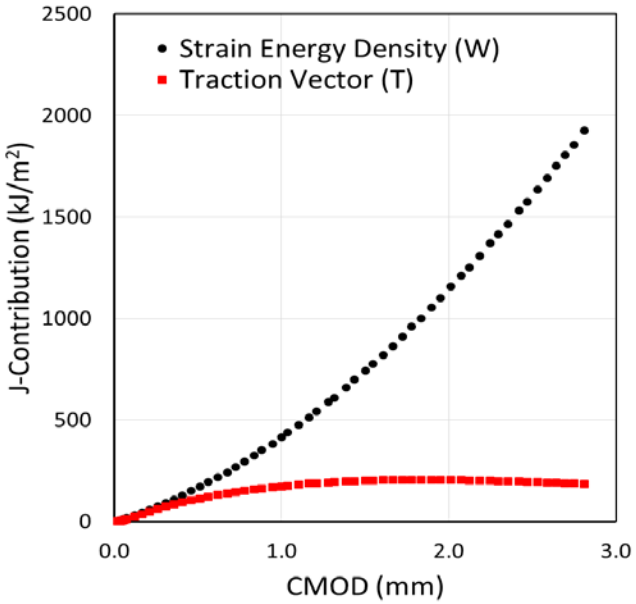

Figure 12. Plot of independent *J*-contributions from both terms in Rice's contour definition of *J* vs. CMOD.

There are a number of methods to obtain the strain contours from the DIC system. The curves of strain vs. position shown in Figure 4, Figure 5 and Figure 6 are all strains calculated by the DIC software for a given value of CMOD. Along with the physical arrangement of the cameras and the speckle coating on the specimen, there are also a number of analysis options that govern how the strains are calculated and ultimately exported for our analysis. Furthermore, how those strains are ultimately used to determine the associated stress can also result in considerable differences.

At this point, readers are cautioned to understand that the data analysis route presented here represents an early attempt at using DIC to obtain *J* values at extremely high strains around the notch. We present our results, including attempts to work around certain issues in our experimental data, for the sake of fostering some critical thinking on this subject. The plots shown in Figure 4, Figure 5 and Figure 6 display smooth curves derived from many individual image correlation operations. While they are used to illustrate simply that there was increasing asymmetry between the strain peaks in the BM, WMC and HAZ respectively, they also resulted in the differences apparent in Figure 8, Figure 9 and Figure 10.

Strain values are available directly from the DIC software, yet in some cases considerable noise was apparent in the exported data, most likely as a result of the speckle patterns, camera resolution, correlation errors and software selectable parameters that can affect the results. This combination of factors implies that the uncertainty reported by the DIC software requires careful scrutiny.

An alternative approach for getting strain values is to export displacements from the DIC system and calculate strain from displacement values, which in most cases had less uncertainty. Arguments can be made for or against any of the options for obtaining strain data, however our intent here is to show the relative effects. Figure 13 shows the differences in *J* calculated using strains calculated by different analysis routes, for each value of CMOD.

Recall from Figure 8 that the $J_{Contour}$ curve presented for specimen J1 showed significant deviation from all of the J_{CMOD} curves; this deviation coincides with the $J_{Contour}$ curve determined from "DIC Strain*" shown in Figure 13. The denoted "DIC Strain*" data includes out of plane and transverse strains that were found to have considerable errors, (e.g. non-physical) and these significantly contributed to the strain energy density, and thus to the relatively high *J* values on this curve.

The strain values obtained from the different methods are the source of the difference and not the determination of stress from strain. To illustrate this, the strain energy density was calculated assuming that the transverse stresses were zero so that the energy density could be determined from ε_{yy} alone without using a Prandtl-Reuss approximation, see data in Figure 13

labeled "DIC Strain eyy only". By use of Prandtl-Reuss with transverse strains, ε_{xx}, and assuming that $\varepsilon_{xx} = -\varepsilon_{yy}/2$, it is clear that the agreement is excellent and is therefore a check that the Prandtl-Reuss approximation is correct.

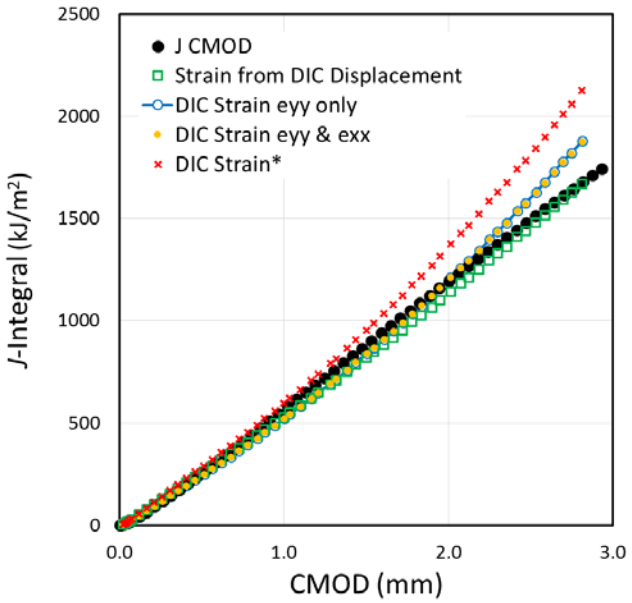

Figure 13. Plot of *J* vs. CMOD showing the relative differences between results derived from different methods of evaluating strain contours. These results are for a single base-metal specimen (J1).

Also recall from Figure 8 that the $J_{Contour}$ curve presented for specimen G1 appeared to track more closely with the J_{CMOD} curves for all the base metal specimens. This result difference was included deliberately again to illustrate another difference in how strain data is derived and treated from the DIC system. In this case, the strains were determined from displacement data. Camera setup and specimen rotation affected the coordinate system assigned by the software and it did not always line up precisely with the specimen edges. This required that the displacement data be transformed to a coordinate system aligned with the specimen boundaries by use of standard vector and strain tensor rotations. Similar rotations of the in-plane strains were carried out. Figure 13 shows the $J_{Contour}$ derived from DIC displacements for specimen J1, which received a similar treatment as G1 did in Figure 8. It is clear that this method of data treatment obtains results more congruent with J_{CMOD} results. However, this method of data treatment is very intensive and a number of intra-method validity checks are necessary.

The next point of discussion is the treatment of strain gradient data for specimens with welds. The placement of the notch in the weld metal centerline or in the heat affected zone will have a significant impact on the strain gradients produced as is evident in Figure 3, Figure 4, Figure 5 and Figure 6. The results presented in Figure 9 were calculated using base metal properties for illustrative purposes, owing to the sensitivity of the results to the material property data used. In the case of Figure 9, all the $J_{Contour}$ curves were determined using strains derived from DIC displacement data as discussed above. It is clear that each of these curves deviate similarly and result in lower *J* values with increasing CMOD when compared to the J_{CMOD} curves for the same specimens.

Examining Figure 5, it is evident that the peak of the strain gradients occur at approximately ± 5 mm about the notch plane. In the case of these specimens which were notched from the root side of the weld (e.g. ID side of the welded pipe), the peak strains on the back-face of the specimens would occur within the weld metal and it follows that weld metal properties should be used to calculate *J*.

Figure 14 shows the new *J* result of a single WMC specimen. Notable here is that by use of weld metal properties, the *J* values shift upward, closer to those obtained by J_{CMOD} which also used weld metal properties.

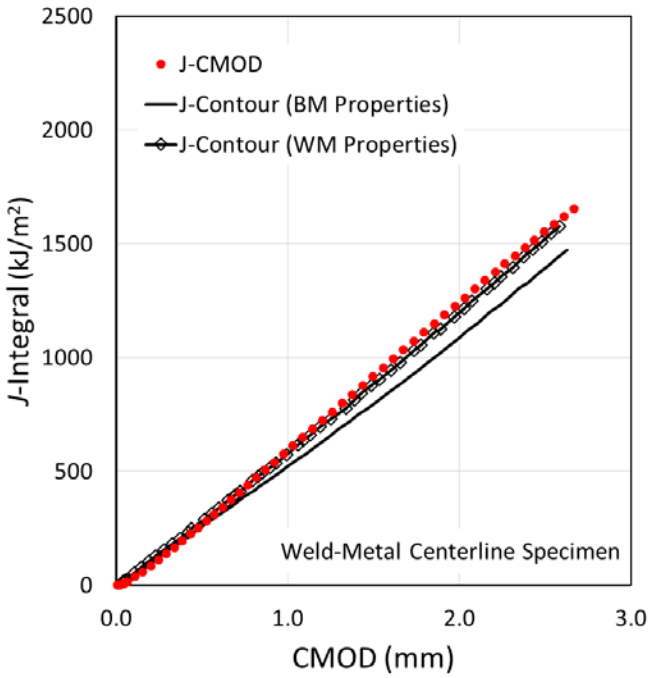

Figure 14. Comparison plot of *J* vs. CMOD for a single specimen notched along the weld-metal centerline. The differences illustrate the effect of using weld-metal properties and base-metal properties.

Up to this point, it is clear that the derivation of strains and how they are used in calculating the strain energy density is the primary contribution to the differences between J_{CMOD} and $J_{Contour}$. The method of determining strain has the largest impact on the shape of the curve *J* vs. CMOD curve, while the material property data has the largest impact on the slope and magnitude of the *J* values.

This is not a surprising result, however examining specimens with notches in the HAZ, the natural progression is to evaluate the strain gradients separately on either side of the notch plane to accommodate different material properties. Caution is warranted with this approach and more analysis is necessary before a conclusion on the appropriate method is determined. The strain gradients shown in Figure 6, indicate an approximate factor of two in the peak strain on either side of the notch plane, for all values of CMOD. However, this factor is not constant and increases with increasing CMOD, suggesting that the contribution to *J* from the smaller gradient is increasing. The smaller of the two gradients is most likely associated with weld metal properties (further increasing *J*). However, the complication using this separation technique is that both strain gradients are a composite of both base-metal and weld-metal strains and are nearly impossible to separate accurately. Figure 15 shows a plot of the results from a single specimen notched in the heat affected zone, calculated by use of base-metal properties and also those calculated from splitting the two gradients and using base-metal and weld-metal properties. This is the simplest method of separating the strain gradients and calculating *J*, but again caution is warranted. Furthermore, as one considers the relative resistance to crack extension, a notch in the heat affected zone would be dominated by base-metal properties with increasing CMOD.

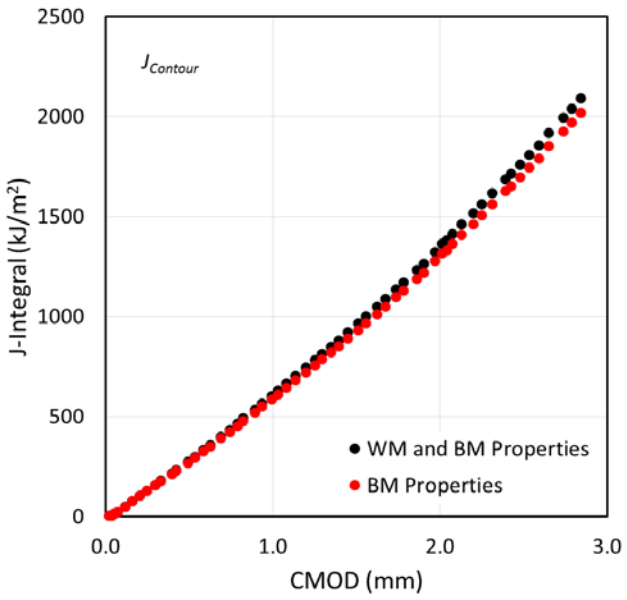

Figure 15. Plot of $J_{Contour}$ vs. CMOD for a single specimen notched in the heat affected zone. The difference in data illustrate the relatively small effect of separating strain contours and calculating the energy density function with different material properties.

The final point of discussion regards the use of only the back-face strain gradients to calculate the strain energy density. Referencing the original work [7], which included strain gradient contributions from both the back-face and front-face, a quick examination of the relative contribution is warranted to satisfy the assertion that the contribution of the front-face strains to *J* is negligible. This was confirmed by examination of the data from the original work but is also presented here using current results.

Figure 16 shows a plot of the integrated strain energy density (first term of Eq. 1) over the length of the specimen as a function of the through-width position, x, for a given value of CMOD. This was calculated for a base-metal specimen but is consistent regardless of notch placement. This plot shows that the contribution of strains at the back-face (x=0 mm) unsurprisingly dominate the energy density value with near zero contribution from strains at the front-face of the specimen (x=14 mm).

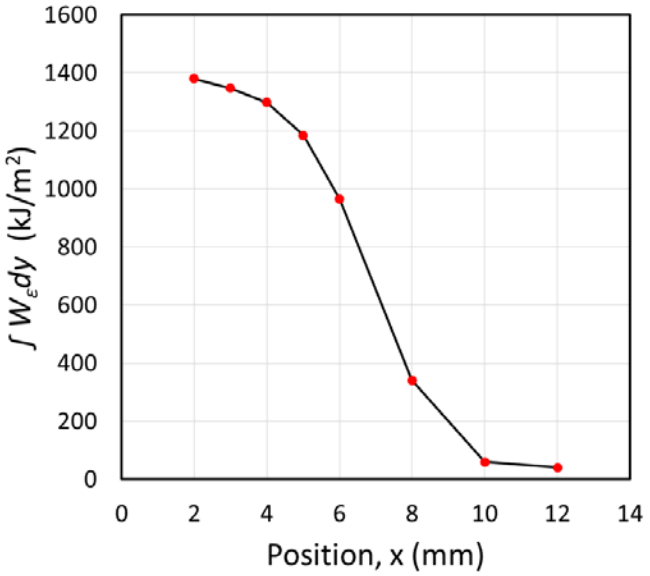

Figure 16. Plot of the integral strain energy density vs. position (through width back-face x=0 mm), derived from the side-face DIC data.

CONCLUSIONS

The results herein represent a small test matrix that involved calculation of the *J*-integral for notched API 5L X65 base- metal, weld metal and the adjacent heat affected zone. The primary purpose of the work was to evaluate a technique to determine the *J*-integral by way of surface strain contours. Determination of *J* from CMOD data is the subject of numerous publications and recommended practices and was used here as a reference for comparison.

The surprisingly good agreement between J_{CMOD} and $J_{Contour}$ shown in Figure 8, Figure 9, Figure 10 and Figure 14 suggest that a useful experimental determination of the *J*-integral for geometries not limited to thoroughly analyzed standard test

structures may be achieved with limited instrumentation, specifically, without use of surface-mounted strain gages, and notably not requiring a determination of crack size nor any instrumentation that requires access to the crack mouth. The determination of crack length for the purpose of generating resistance (R) curves is deliberately absent this work. Our intent is to first compare experimental estimates of *J* on well controlled experiments and geometries. Furthermore, the determination of crack size has uncertainty superimposed on J_{CMOD} and subsequently on *J*-R; more work is necessary to examine this impact on comparisons.

We used the applied force from the load cell of the testing machine to obtain the traction-bending term of $J_{Contour}$; however, Figure 12 shows that this term is much smaller than the energy density term, so improvements in DIC techniques may permit its evaluation with sufficient accuracy from DIC data alone. Additionally, analysis of multiple strain contours to include very large contours will be held as future work. The traction-bending term could theoretically approach zero with sufficient distance from the crack, however, within the physical limitations of these specimens the contribution gradually decreases but does not achieve zero. Furthermore, future work and analysis with respect to path independence with multiple contours is necessary.

The following salient conclusions can be drawn from the Results and Discussion sections:

- Back-face strain gradients provide adequate data to determine the *J*-integral with negligible contributions from front-face strains; the traction-bending term is small but not negligible;
- Digital image correlation provides sufficient full-field strain data for use by this method and is considerably more robust than surface-mounted strain gage instrumentation;
- Caution must be exercised with respect to the strains exported from commercially available DIC analysis software;
- Validity checks presented to select the appropriate strain data treatments, specifically the axial strains, ε_{yy} have been determined to give the best and technically defensible strains for the technique;
- Strains derived from displacement data produce results most congruent with the J_{CMOD} reference data, yet require intensive rotation corrections;
- Strain contours are the primary contribution to the *J*-integral, with a secondary contribution from material properties used to calculate the strain energy density;
- The strain contours associated with different material properties in a welded specimen require careful use of the appropriate local material properties but the contributions of multi-property contours are nearly impossible to separate;
- Prandtl-Reuss approximations were demonstrated to be feasible even with relatively large deformations. However, our DIC data contained strain errors of the order of the yield strain, which were capable of causing our solution method for the Prandtl-Reuss equations to produce non-physical stress values.

ACKNOWLEDGMENTS

Funding for this research was provided by the U.S. Department of Commerce, National Institute of Standards and Technology's Pipeline Safety Project. The authors are grateful to L.N. Pussegoda and S. Tiku at BMT Fleet Technology Ltd. for providing test specimens used for this research.

REFERENCES

1. BS-8571, *Method of Test for Determination of Fracture Toughness in Metallic Materials Using Single Edge Notched Tension (SENT) Specimens.* 2014, British Standards Institution.
2. CanmetMATERIALS, *Recommended Practice: Fracture Toughness Testing Using SE(T) Samples With Fixed-Grip Loading*. Report No. 2010-31(TR), 2010.
3. E1820-15a, *Standard Test Method for Measurment of Fracture Toughness*. 2015, ASTM International.
4. ExxonMobil, *Measurement of Crack Tip Opening Displacement (CTOD) - Fracture Resistance Curves Using Single-Edge Notched Tension (SENT) Specimens*. 2010.
5. DNV-RP-F108, *Recommended Practice: Fracture Control for Pipeline Installation Methods Introducing Cyclic Plastic Strain*. 2006, Det Norske Veritas.
6. Weeks, T.S. and E. Lucon. *Direct Comparison of Single-Specimen Clamped SE(T) Test Methods on X100 Line Pipe Steel*. in *International Pipeline Conference*. 2014. Calgary, Alberta, Canada: ASME.
7. Weeks, T.S. and D.T. Read. *Comparison of J-integral from single specimen SE(T) tests on API-5L X100 line pipe steel*. in *International Ocean and Polar Engineering Conference*. 2015. Kona, HI, USA: ISOPE.
8. Yoneyama, S., S. Arikawa, S. Kusayanagi, and K. Hazumi, *Evaluating J-integral from Displacement Fields Measured by Digital Image Correlation.* Strain, 2014. **50**(2): p. 147-160.
9. Becker, T., M. Mostafavi, R. Tait, and T. Marrow, *An Approach to Calculate the J-integral by Digital Image Correlation Displacement Field Measurement.* Fatigue & Fracture of Engineering Materials & Structures, 2012. **35**(10): p. 971-984.
10. Fagerholt, E., E. Østby, T. Børvik, and O. Hopperstad, *Investigation of Fracture in Small-Scale SENT Tests of a Welded X80 Pipeline Steel Using Digital Image Correlation with Node Splitting*. Engineering Fracture Mechanics, 2012. **96**: p. 276-293.

11. Verstraete, M., R. Denys, K. Van Minnebruggen, S. Hertelé, and W. De Waele, *Determination of CTOD Resistance Curves in Side-Grooved Single-Edge Notched Tensile Specimens using Full Field Deformation Measurements.* Engineering Fracture Mechanics, 2013. **110**: p. 12-22.
12. Hertelé, S., M. Verstraete, K. Van Minnebruggen, R. Denys, and W. De Waele. *Applications of Digital Image Correlation in Girth Weld Testing*. in *6th International Pipeline Technology Conference*. 2013. Soete Laboratory.
13. Shen, G., J.A. Gianetto, and W.R. Tyson, *Development of Procedure for Low-Constraint Toughness Testing Using a Single-Specimen Technique*, in *MTL Report No. 2008-18 (TR)*. 2008, CanmetMATERIALS.
14. Cravero, S. and C. Ruggieri, *Estimation Procedure of J-Resistance Curves for SE(T) Fracture Specimens Using Unloading Compliance*. Engineering Fracture Mechanics, 2007. **74**(17): p. 2735-2757.
15. Rice, J.R., *A Path Independent Integral and the Approximate Analysis of Strain Concentration by Notches and Cracks.* Journal of Applied Mechanics, 1968. **35**(2): p. 379-386.